Journal Name

ARTICLE

Comparison of bulk and microfluidic methods to monitor the phase behaviour of nanoparticles during digestion of lipid-based drug formulations using *in situ* X-ray scattering

Received 00th January 20xx,
Accepted 00th January 20xx

DOI: 10.1039/x0xx00000x

www.rsc.org/

Linda Hong,[a,b] Muhsincan Sesen,[c,f] Adrian Hawley,[d] Adrian Neild,[c] Patrick T. Spicer[e] and Ben J. Boyd[a,b]*

The performance of orally administered lipid-based drug formulations is crucially dependent on digestion, and understanding the colloidal structures formed during digestion is necessary for rational formulation design. Previous studies using the established bulk pH-stat approach (Hong *et al*. 2015), coupled to synchrotron small X-ray scattering (SAXS), have begun to shed light on this subject. Such studies of digestion using *in situ* SAXS measurements are complex and have limitations regarding the resolution of intermediate structures. Using a microfluidic device, the digestion of lipid systems may be monitored with far better control over the mixing of the components and the application of enzyme, thereby elucidating a finer understanding of the structural progression of these lipid systems. This work compares a simple T-junction microcapillary device and a custom-built microfluidic chip featuring hydrodynamic flow focusing, with an equivalent experiment with the full scale pH-stat approach. Both microfluidic devices were found to be suitable for *in situ* SAXS measurements in tracking the kinetics with improved time and signal sensitivity compared to other microfluidic devices studying similar lipid-based systems, and producing more consistent and controllable structural transformations. Particle sizing of the nanoparticles produced in the microfluidic devices were more consistent than the pH-stat approach.

Introduction

Amphiphilic molecules can self-assemble into a variety of different liquid crystalline geometries, such as cubic or hexagonal phases, when hydrated with solvent.[1] Dispersions of lipidic liquid crystalline phases consist of sub-micron particles that possess the internal phase structure comprising ordered internal hydrophilic and hydrophobic channels.[2] When the bicontinuous cubic (V_2) and inverse hexagonal (H_2) phases are dispersed in excess solvent, the particles are known as cubosomes and hexosomes, respectively. Transitions between structures can be triggered using various stimuli such as temperature,[3] enzymes,[4–6] changes in pH,[7,8] addition of guest molecules (eg. DNA, cyclodextrins)[9–11] or a change in ionic strength.[12–14] In drug delivery applications, different phases can exhibit different rates of drug release.[15,16] Thus, there is an opportunity to take advantage of these transformations to control the rate and location of drug availability.

There is a growing recognition that lipid self-assembly during digestion may be crucial to determining interactions with drugs,[17] drug absorption and overall effectiveness of lipid-based drug formulations and that it could be used to deliberately target specific structural transformations in the gut. Fong *et al*. and Hong *et al.* designed enzyme-responsive lipid-based systems to trigger the structural evolution from a slow-releasing micellar phase structure to a fast-releasing cubic structure.[4,5] Synchrotron-based small angle X-ray scattering (SAXS) coupled to an *in vitro* digestion model, known as the pH-stat approach, (Fig. 1A) was employed to monitor the structural transformations in real time.[18]

The initially unstructured emulsion (inverse micellar L_2 phase in Fig. 1B) consisted of the lyotropic lipid phytantriol mixed with a bulky triglyceride, such as tributyrin (Fig. 1C). When together, the triglyceride disrupts the natural tendency of the phytantriol to form the bicontinuous cubic phase. For an emulsion consisting of phytantriol and tributyrin, the scattering initially provided only a broad hump which shifted to the left of the profile as the lipids were digested with the addition of enzyme at 200 secs (Fig. 1B). This implies that the lattice parameter, which can infer the internal water channel dimension, had increased. The hump gradually lessened in prominence during digestion as peaks with a spacing ratio of √2, √3, √4, √6, √8, √9 emerged. This specific scattering profile is unique to the bicon-

[a] Drug Delivery, Disposition and Dynamics, Monash Institute of Pharmaceutical Science, Monash University (Parkville Campus), 381 Royal Parade, Parkville, VIC 3052, Australia
[b] ARC Centre of Excellence in Convergent Bio-Nano Science and Technology, Monash Institute of Pharmaceutical Sciences, Monash University (Parkville Campus), 381 Royal Parade, Parkville, VIC 3052, Australia
[c] Department of Mechanical and Aerospace Engineering, Monash University, Clayton, VIC 3800, Australia.
[d] SAXS/WAXS Beamline, Australian Synchrotron, 800 Blackburn Rd, Clayton, VIC 3150, Australia
[e] School of Chemical Engineering, University of New South Wales, Sydney, NSW 2052, Australia
[f] Present address: Department of Bioengineering, South Kensington Campus, Imperial College London, SW7 2AZ, United Kingdom.
† Electronic Supplementary Information (ESI) available online. See DOI: 10.1039/x0xx00000x

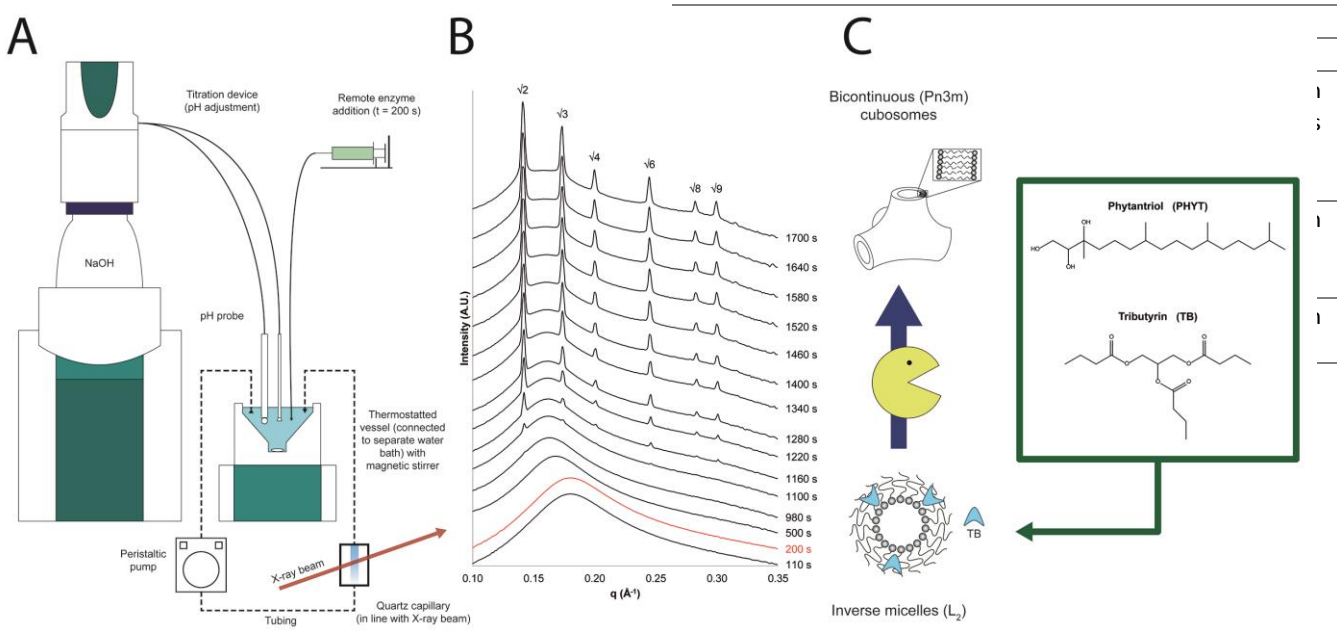

Fig. 1 A) The experimental configuration for the pH-stat approach integrated with the X-ray beam for SAXS measurements. There are multiple components to the configuration to control parameters such as temperature and pH. B) A set of scattering profiles following the kinetics of the structural evolution during the digestion of a lipid system, showing the transformation from inverse micelles to cubic phase particles after the addition of enzyme at 200 secs. The annotation of the peaks with their relative spacing ratios as √2, √3, √4 etc. indicates the presence of the highly ordered cubic phase, forming from the disordered L_2 phase indicated by the broad hump. Figure adapted with permission from Hong *et al.*[5] Copyright 2015 American Chemical Society. C) A schematic of the enzyme-induced transformation from the inverse micelle containing phytantriol (PHYT) and tributyrin (TB).

tinuous cubic *Pn3m* phase, which is the structure that phytantriol self-assembles into at these conditions.[19] No apparent intermediate phases were observed.[5]

Although the pH-stat approach allows tracking of the phase transitions over time, the experimental apparatus required is cumbersome and difficult to incorporate with advanced analytical techniques. The pH-stat apparatus, schematically presented in Fig. 1A, requires at least 20 mL volume to run in flow through mode, which can be prohibitive for investigating special lipid compositions, or where drugs are incorporated into the materials. There is also a delay in formulation transiting from the digestion vessel to the capillary, during which phase transitions are possible. The mixing efficiency inside the vessel is also not well understood. Lastly, the means of remote delivery of the enzyme to the vessel via a syringe driver, means that at early time points there is a non-homogeneous distribution of lipase, presenting uncertainty about non-equilibrium structures and non-uniform compositions. Ideally, the sample should be examined instantaneously once fully mixed. The advantages of microfluidics over the bulk approach has been summarised in Table 1.

Table 1. Summary of the advantages and the limitations of the bulk pH-stat approach versus the microfluidics approach.

To reduce the experimental space required by the apparatus, greatly enhance mixing control, decrease sample consumption, and enable *in situ* analysis of transformations, microfluidics is proposed as an alternative format to alleviate the shortcomings of the pH-stat approach.[20] The ability to monitor real-time transformations along the microchannel is a result of the low Reynold's number.[21] This yields laminar flow and diffusion-limited mixing, thus allowing the correlation between the spatial position in the microchannel and the temporal position in the reaction.[22,23] Additionally, microfluidics can demonstrate a higher sensitivity, improved reproducibility, and be used as a high throughput method,[20] all of which can be advantageous for these studies.

Microfluidic approaches have been previously applied to assist the analysis of lipid-based systems with conventional techniques.[24] The incorporation of DNA into multilamellar vesicles by Otten *et al.* was determined by a change in the *d*-spacing (spacing between two aligned lattice planes) of the DNA interaxial distance which could be detected with SAXS.[25] The kinetics of this change were monitored along the length of a microfluidic channel where an intersection of three converging channels resulted in the co-axial flow of a DNA solution between two streams containing vesicles. The design of the channels is generalised in Fig. 2. More recently, Ghazal *et al.* monitored a lipidic cubic phase system changing from the *Im3m* phase to the *Pn3m* phase when mixed with calcium ions using a similar channel design.[12] The point of complete diffusion of the ions into the formulation could also be characterised with equations taking into account flow rates and the diffusion coefficient of the substrates among other variables. In both instances, the three co-axial streams allowed diffusion of a stimuli-inducing substance via two interfaces into the stream of the formulation to yield a

structural change.

Ghazal *et al.* and Otten *et al.* performed their experiments using custom microfluidic chips, however these facilities may not be readily accessible to all researchers. While microfluidic devices can be made incredibly complex, simpler "off-the-shelf" devices have been used to achieve similar manipulations of liquid crystal systems.[26,27] A simple T-junction configuration composed of liquid chromatography components was utilized by Bottaro *et al.* to form and load liposomes.[26] The results were compared with equivalent experiments in a chip-based microfluidic device and with the bulk approach.[26] Size dispersity was observed to be more consistent and lower for the "off-the-shelf" device, which is particularly important for drug delivery applications.

Consequently in this work, the practicalities of an "off-the-shelf" and chip-based microfluidic device to study the digestion of lipid-based formulations were investigated. The configuration of the channels in either device can enable laminar flow for the solutions of enzyme and formulations alongside each other. The custom-fabricated microfluidic chip to study the digestion of lipid-based formulations was fabricated taking into account the elements identified in the devices from Ghazal *et al*. and Otten *et al*.[12,25] Digestion would occur due to diffusion between the enzyme and formulation streams, affording more control over the transformation than former methods. However, the suitability of either device is anticipated to depend on the channel design, flow rate limits, and the compatibility with SAXS.

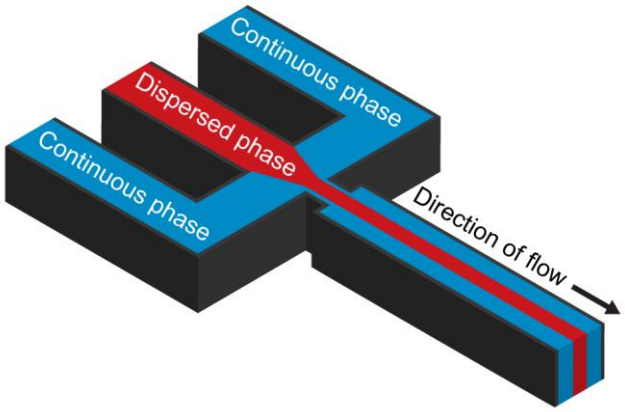

Fig. 2 Schematic of the channel design used to converge three incoming channels known as hydrodynamic flow focusing. The three flows enter the output channel where the flow of the dispersed phase is sandwiched by the two flows of the continuous phase. There are two interfaces through which substrates can diffuse across for reactions to occur.

In contrast to traditional pH stat studies where the sample was analysed at a fixed position under a flow-through apparatus, different positions along the channel in the microfluidic devices were successfully aligned with the SAXS beam to allow acquisition of the structural data correlating to different time points in the reaction. The total flow rates (TFR) were manipulated to alter the kinetics of the digestion and enable the observation of the full transition of the stimuli-responsive formulation. Data were then compared to the phase behaviour observed with the pH-stat approach. Two enzyme-sensitive emulsions were examined: phytantriol with 20% w/w tributyrin (PHYT20TB) and phytantriol with 15% w/w tricaprylin (PHYT15TC), selected based on previous studies with these systems.[5] Specifically, the PHYT20TB emulsion was reported previously to transition from the L_2 phase to the cubic *Pn3m* phase with no intermediate phases observed in the pH-stat approach. The PHYT15TC system transitioned from the L_2 phase to the H_2 phase to the bicontinuous cubic *Pn3m* phase. The PHYT20TB system is a well-studied system and a good test case for microfluidics interfacing with SAXS, while the digestion of PHYT15TC is of interest for its transformation across three phases.

Materials and Methods

Phytantriol (3,7,11,15-tetramethylhexadecane-1,2,3-triol, PHYT) was from DSM Nutritional Products Ltd, Singapore. Selachyl alcohol (SA) was obtained from Hai Hang Industries, China. Tributyrin (TB) and tricaprylin (TC) were obtained from TCI Chemicals, Tokyo, Japan. Sodium chloride was from Chem-Supply, SA, Australia. Trizma maleate, butyric acid (BA), caprylic acid (CA) and 1-monocaprylоyl-rac-glycerol (C8:0, MC) were obtained from Sigma-Aldrich, MO, U.S.A. Calcium chloride dihydrate and glycerol (GLY) were from Ajax Finechem, NSW, Australia. Sodium azide was from Merck Schuchardt OHG, Darmstadt, Germany. Sodium hydroxide pellets were from Ajax Chemicals, NSW, Australia. Water was from a Milli-Q water purification unit (Millipore, Australia). Synperonic F108 (Pluronic F108) was purchased from Fluka, France. Pancreatin was obtained from Southern Biological, VIC, Australia. 4-bromophenylboronic acid (4-BPBA) was acquired from Aldrich, China. Methanol was obtained from Merck KGgA, Darmstadt, Germany. All chemicals were used without further purification.

Sample preparation

Digestible lipid formulations. In a scintillation vial (20 mL), phytantriol was combined with TB (20% w/w of lipid content) or TC (15% w/w of lipid content). The lipid mixtures were heated

until they flowed at 60°C and vortexed until homogeneous. Lipid (10% w/w) was then dispersed in a Tris buffer solution (containing 1% w/w Pluronic F108) using a Misonix Ultrasonic liquid processor S-4000 (USA) at 30% amplitude for 2.5 min, pulsing on for 4 secs and off for 1 sec. Tris buffer at pH 6.5 was comprised of the following: 150 mM sodium chloride, 50 mM Trizma maleate, 5 mM calcium chloride dihydrate, 6 mM sodium azide, and 50 mM sodium hydroxide.

Static simulated 'digested' lipid formulations. Different proportions of the phytantriol, triglyceride and digestion products (fatty acids and monoglyceride or glycerol) were dispersed in Tris buffer containing 1% Pluronic F108 and processed as described with the aforementioned formulations. Each formulation contained the same amount of phytantriol with the remainder of the lipid component comprised of required amounts of triglyceride and digestion products. As the amount of triglyceride was decreased in the formulation, the equivalent mass was replaced by the appropriate mol ratios of the fatty acid and monoglyceride or glycerol. To determine the compositions of the simulated 'digested' formulations, it was assumed that TB was digested to yield a 1:3 glycerol:fatty acid mol ratio,[28] while TC digested to a 1:2 monocaprylin:caprylic acid mol ratio.[29] The compositions of each formulation have been described in Supplementary table 1 and Supplementary table 2 for PHYT20TB and PHYT15TC, respectively.

Enzyme suspension. A lipase suspension was rehydrated from a freeze-dried preparation of pancreatic lipase with Tris buffer (containing 1% w/w Pluronic F108) prepared according to the method described by Clulow *et al.*[30] Activity was determined to be 500 TBU/mL of digest.

Equilibrium phase behaviour

The static simulated 'digested' lipid formulations were loaded into quartz capillaries for SAXS measurements at the Australian synchrotron. The formulations were analysed using an X-ray wavelength λ = 0.954 Å (equivalent to energy = 13 keV) and a sample to detector distance of 1531 mm (determined by calibration with silver behenate) which provided a q range of 0.0111 - 0.659 Å^{-1}, where q is the scattering vector determined by the equation: $q = 4\pi/\lambda \sin(\theta/2)$, where θ is the scattering angle. Acquisition time at the detector was set to 5 secs. The two-dimensional scattering patterns were acquired using a Pilatus 1M detector with an active area of 169 × 179 mm^2 with 172 µm pixel size. The scattering patterns were then integrated into a one-dimensional scattering function I(q) using the in-house software, Scatterbrain (version 1.15).[31]

Identification of the nanostructures from the scattering function was determined by correlating the relative spacing ratios between the positions of the Bragg peaks to literature.[32]

Microfluidic setup

"Off-the-shelf" microfluidic device (OTS-MF). The capillary-based microfluidic device was assembled using a T-junction (IDEX P-728 PEEK Tee with a 1.3 mm thru-hole) and a borosilicate glass capillary (1.5 mm OD, 0.84 mm ID, length: 100 mm, World Precision Instruments, U.S.A.) as shown in Fig. 3. The capillary was fitted securely into the T-junction with approxi-

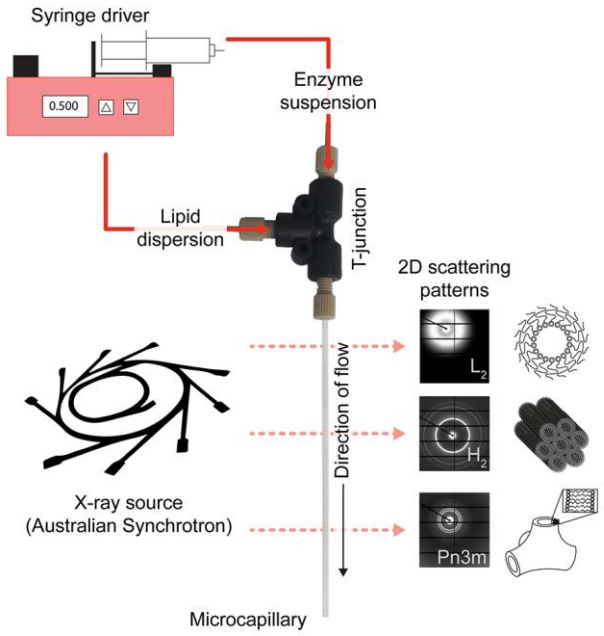

Fig. 3 Schematic of the off-the-shelf microfluidic (OTS-MF) setup in line with the X-ray beam at the SAXS beamline (Australian Synchrotron). Solutions were delivered to the T-junction via a syringe driver before flowing into the capillary. The X-ray beam scanned the length of the capillary to track the structural kinetics of the digestion.

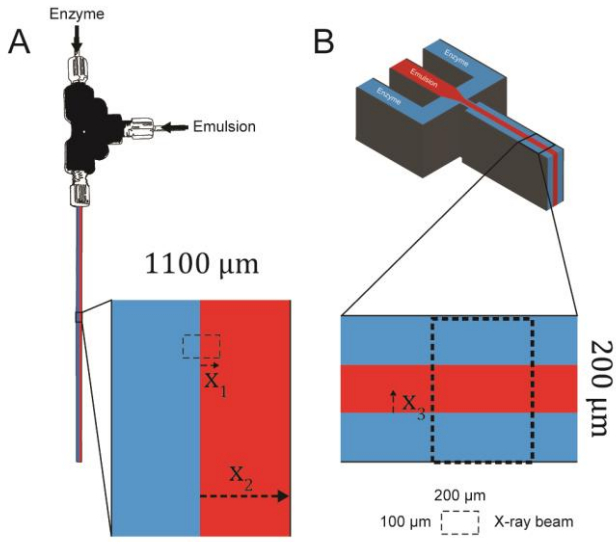

Fig. 4 Schematic depicting the distance, x, the enzyme in the blue stream needs to traverse across the flow of the emulsion (red) to be considered fully mixed in the two microfluidic devices. A) The enzyme needed to travel 420 µm, which was half the width of the capillary of the OTS-MF device (x_2) to access all droplets in the emulsion. However, given the X-ray beam was only 200 µm in width and focused at the centre of the channel, calculations only needed to take into account half this dimension (x_1). B) As there were two streams of enzyme on either side of the stream of emulsion, enzyme only needed to travel to the centre of the enzyme flow (x_3) to be considered fully diffused.

mately 7 cm of the length accessible to the X-rays. The solutions to be mixed were filled in separate Luer Lock syringes (3 mL) and

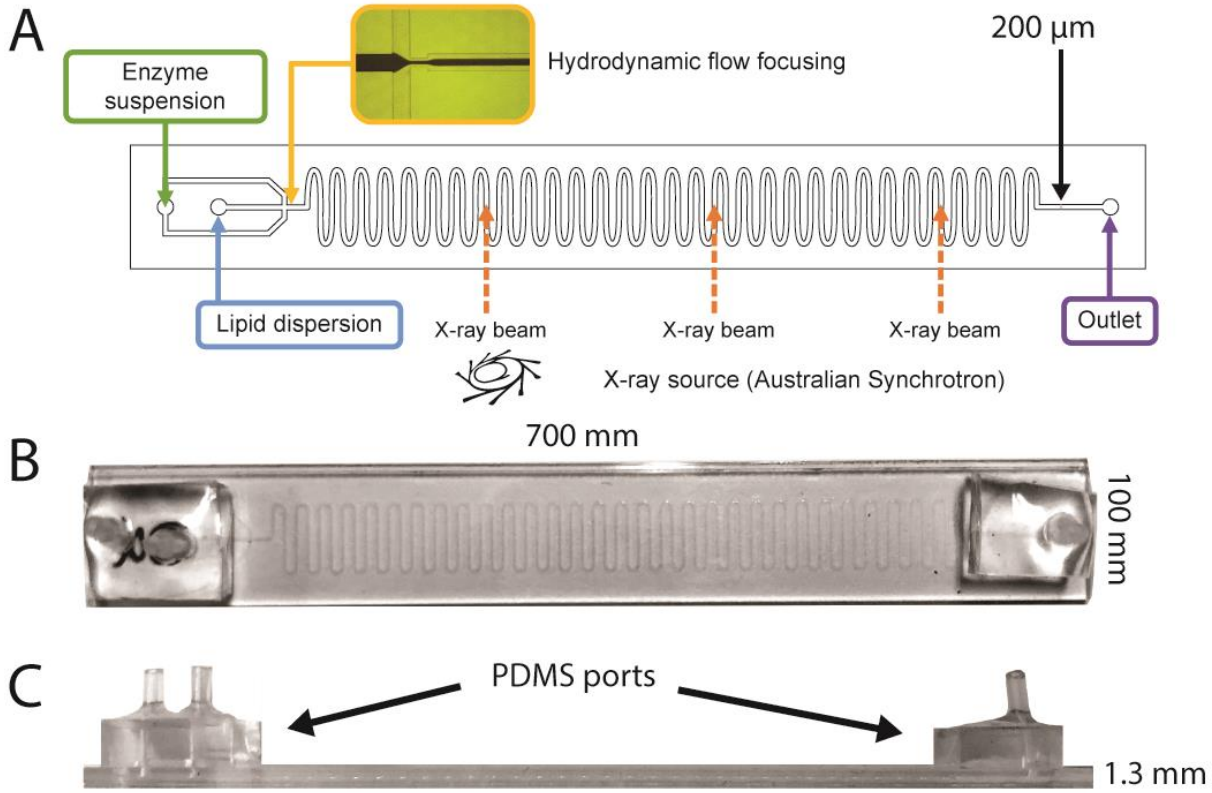

Fig. 5 A) Diagram of the serpentine microfluidic (S-MF) device and how it was used in line with SAXS. The enzyme solution and lipid dispersion were delivered to the inlet channels on the left via syringe pump. When the solutions converged at the intersection, the enzyme solution pinched the lipid dispersion to form a co-flow of solutions known as hydrodynamic flow focusing (inset). The X-ray beam was focused at various positions along the microchannel to track the kinetic nanostructures by mounting the chip and syringe drivers on an XYZ translation stage with the chip perpendicular to the beam. B) Top view of the device. C) Side view of the device. There were three ports in which the tubing can be inserted to deliver the solutions into the channels (left) or remove waste (right).

delivered to the T-junction via HPLC tubing. Fittings (NanoTight™ PEEK Headless, Short, 10-32 Coned, for 1/16" OD) from IDEX Health and Science (USA) were used to connect the tubing to the T-junction, and the T-junction to the capillary. Both syringes were controlled using the NE-4000 2 Channel Syringe Pump from New Era Pump System Inc. (U.S.A.).

Serpentine microfluidic device (S-MF). The custom microfluidic device illustrated in Fig. 5 was fabricated at the South Australian node of the Australian National Fabrication Facility. The device featured microchannels etched into quartz to a depth of approximately 60 µm. The channel design included two inlet channels where one inlet port divided into two channels and converged at the intersection with the other inlet channel. Flow proceeded through a serpentine length of channel of length ~350 mm before exiting from the outlet port. Two syringes (1 mL, from BD, U.S.A.) driven by a syringe driver as described for OTS-MF delivered the solutions to the device via PTFE tubing (0.012"ID x 0.030"OD, Cole-Parmer, U.S.A.).

Monitoring the real-time evolution of structure during digestion

In the microfluidic devices. Structural kinetic studies were performed on the SAXS/WAXS beamline at the Australian Synchrotron, VIC, Australia.[33] The microfluidic devices were fixed to a metal support, with the microchannels positioned in-line with the X-ray beam. The enzyme suspension and lipid formulation were flowed to the devices via the syringe driver at a flow rate ratio of 1 and variable TFR. The system was stabilized for an appropriate amount of time before structural data were acquired. Data were acquired at consistent increments along the length of the microchannels, noting the exact locations to determine the corresponding reaction time points. Experiments were run at hutch temperature (~27 °C).

The scattering experiments conducted with the OTS-MF device utilised the setting described previously in **Equilibrium phase behaviour**. The S-MF device in other experiments required a wavelength of 0.620 Å (20 keV) with sample to detector distance of 1561 mm which provided a q range of 0.0193 - 0.611 $Å^{-1}$. Acquisition time of the data was set to 30 secs. Once more, the scattering patterns were then integrated into a one-dimensional scattering function I(q) using the in-house software, Scatterbrain (version 1.15).[31] Identification of the nanostructures from the scattering function was determined by correlating the relative spacing ratios between the positions of the Bragg peaks to literature.[32]

In the pH-stat apparatus. To compare with microfluidic experiments, equivalent experiments were run with the pH-stat apparatus. The pH-stat apparatus was set up to digest 1 mL of

formulation with 1 mL of enzyme, and the mixture diluted to 17 mL with Tris buffer to facilitate a flow-through digestion as described by Warren *et al.*[18] The settings for SAXS were the same as for the OTS-MF device. Digestions were run at 37 °C, while the pH was maintained at 6.5 with automated titration (0.2 M NaOH). Once digested to completion at 380 secs, 1 mL of the digested PHYT20TB solution was added to 10 µL of 5 mg/mL 4-BPBA in methanol for particle size testing.

Determination of the completion of diffusive mixing

The digestion of the lipid in the microfluidic devices was limited by the diffusion of the enzyme at the lipid-enzyme solution interface to the far edge or centre of the lipid stream for the OTS-MF and S-MF devices, as represented by x_2 and x_3 respectively in Fig. 4. To determine the position of complete diffusion along the microchannel, the time of complete mixing, *t*, was first calculated using Equation 1.[12,34]

Equation 1. Equation to determine the time of complete mixing across a distance, *x*, and taking into account the diffusion coefficient, *D*.

$$t = {x^2}/{2D}$$

This equation takes into account the lateral distance the solute, *x*, in this case is lipase, must travel across (which has been illustrated in Fig. 4), and its diffusion coefficient, *D*. For the OTS-MF device, the distance that the enzyme needed to diffuse across was 100 µm which is half the width of the X-ray beam and the only relevant region for calculating the diffusion. The diffusion coefficient of the pancreatic lipase was obtained from literature[35] and adjusted for Taylor-Aris dispersion using Equation 2.[36]

Equation 2. Equation used to adjust the diffusion coefficient of molecules, taking into account the Taylor-Aris dispersion, where K is the Taylor-Aris dispersivity, U is the average fluid velocity, and d is the distance between the parallel walls of the microfluidic channels.

$$\frac{K}{D} = 1 + \frac{1}{210}\left(\frac{Ud}{D}\right)^2$$

The complete mixing time was then converted to a distance along the length of the microchannel. The average velocity was determined from the flow rates and the volume of the channels. An example of these equations used for the total flow rate of 1200 µL/hr can be found in Supplementary table 3. The distance at which complete diffusion is expected with adjusted diffusion coefficients for the pancreatic lipase are shown in Supplementary table 4 and Supplementary table 5 for the OTS-MF and S-MF device, respectively.

Comparing particle size between the pH-stat and microfluidic techniques

Dynamic light scattering (Zetasizer Nano ZS, Malvern Instruments, UK) was performed on samples obtained from the end point of digestion of PHYT20TB in the microfluidic devices at different TFR. The digested sample was collected (2 µL), diluted in 995 µL of Milli-Q-grade water and run immediately without inhibitor. Experiments were run in triplicate. Inhibited samples collected from the pH-stat digestions were also assessed with the same protocol.

Results and discussion

The use of microfluidics in conjunction with traditional analytical techniques to investigate the transformations of enzyme-responsive liquid crystalline systems can enable greater control over experiments. Microfluidics can also be customized to achieve any experimental manipulations through alterations in channel designs, material or the device, or additional electronic components. Due to the numerous available customizations and their vast range in costs for fabrication, the results were used to compare a relatively inexpensive OTS-MF device with the S-MF device. Factors including mixing efficiency, signal resolution (SAXS) and particle sizing were evaluated between the devices.

Influence of the microfluidic design for mixing

Channel design determines the flow of solutions and mixing efficiency in microfluidic devices. The OTS-MF device featured a T-junction allowing the convergence of the lipid formulation and enzyme suspension. The two solutions flowed as two streams along the length of the capillary. As such, enzyme could only diffuse through one interface of the lipid stream to induce digestion. The S-MF device featured three converging channels that resulted in hydrodynamic flow focusing and the co-axial flow of three streams (lipid emulsion sheathed by two enzyme streams).[12,22] This provided relatively more interfacial area through which the enzyme can diffuse.

The position of complete mixing relative to the full length of the respective microchannels was calculated to occur earlier along the channel for experiments in the S-MF device than in the OTS-MF device, and slower TFR were calculated to delay the diffusion process (refer to Supplementary Table 4 & 5). At the slowest TFR (10 µL/hr) used in the S-MF device, complete diffusion was calculated to occur by 8% of the entire length of the channel (28 mm from the point of initial contact) while complete mixing was anticipated to occur by 2% of the channel length at 40 µL/hr (7 mm from the point of initial contact). A similar trend was calculated for the OTS-MF device where shorter distances of complete diffusion were calculated for faster TFR (0.14% of the channel when set to 12000 µL/hr), and vice versa longer distances were calculated for slower TFR (14.4% of the channel when set to 120 µL/hr). The greater flow rates enhanced the Taylor-Aris dispersion effect and consequently the diffusion coefficient of the lipase (refer to Equation 2). As such, the position of complete diffusion into the lipid stream was calculated to occur earlier along the channel. Although the distance to complete mixing in the OTS-MF device was at most 14.4 mm from the point of convergence, this distance was within the section of capillary hidden in the T-junction and inaccessible to X-rays (or other analytical techniques), therefore data obtained at all positions along the remaining length of the capillary reflected completely mixed systems, and any non-equilibrium structures would not be due to incomplete mixing. As for the S-MF device, the position of complete mixing occurred within the first 8% of the channel, leaving more than 32 cm of the channel available for tracking phase transitions.

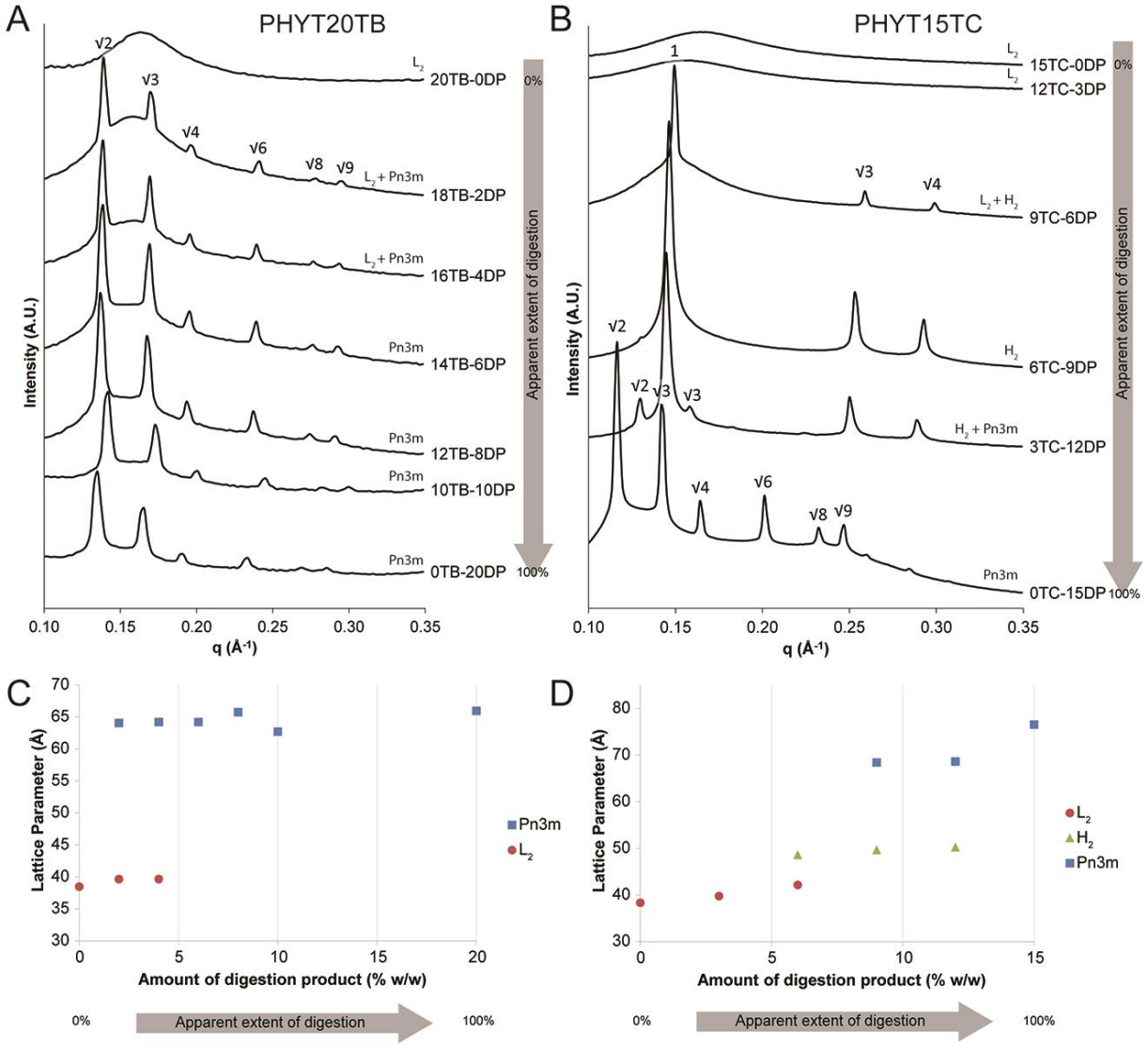

Fig. 6 Phase diagrams of different compositions of the formulations with % w/w triglyceride (tributyrin: TB; tricaprylin: TC) and % w/w digestion product (DP). Each formulation simulated the composition of the digested formulation at various stages of hydrolysis of the triglyceride showing the apparent extent of digestion of the enzyme-sensitive emulsions. A) An emulsion containing phytantriol with 20% w/w tributyrin (PHYT20TB) transitioned from L_2 phase to cubic *Pn3m* phase at 18% w/w TB (18TB-2DP), and B) An emulsion containing phytantriol with 15% w/w tricaprylin (PHYT15TC) transitioned from L_2 phase to H_2 phase and finally cubic *Pn3m* phase upon complete replacement of TC with digestion products of the triglyceride (0TC-15DP). The data is also plotted as a lattice parameter vs. the amount of digestion product in the system in C) for the TB system and in D) for the TC system.

Phase diagram of samples representing equilibrium compositions expected during 'digestions'

The structure of samples at specific compositions representing different stages of digestion were measured using SAXS to compare to the structures formed during the dynamic digestion experiments (Fig. 6). The relative spacing between the peaks was used to determine the different phases and the lattice parameters of the different structures were also calculated over the apparent extent of 'digestion'.

Each formulation comprised of the same amount of structure forming lipid, PHYT, and varying amounts of triglyceride and/or the digestion products (DP). The DP were comprised of the fatty acids and monoglycerides or glycerol in their appropriate mol ratios. The ratio of triglyceride to DP was varied to represent different extents of digestion and was described in Supplementary table 1 and Supplementary table 2.

Without any digestion products being present, i.e. the starting formulation at time = 0, the PHYT20TB emulsion was in the L_2 phase as demonstrated by the broad hump (20TB-0DP) in Fig. 6A. In the case of the PHYT20TB system, the DP consisted of 3 mol of butyric acid and 1 mol glycerol. At 18% w/w TB and 2% w/w DP (18TB-2DP), peaks with a spacing ratio of √2, √3, √4, √6, √8, √9 in coexistence with the emulsion were apparent, signifying the presence of the ordered cubic *Pn3m* phase. As the proportion of triglyceride was replaced by fatty acids and glycerol/monoglycerides, the characteristic hump became more level with the background scattering while the peaks for cubic phase became more pronounced, signifying a clear range of concentrations over which the system transitioned from L_2 phase to the bicontinuous cubic phase structure.

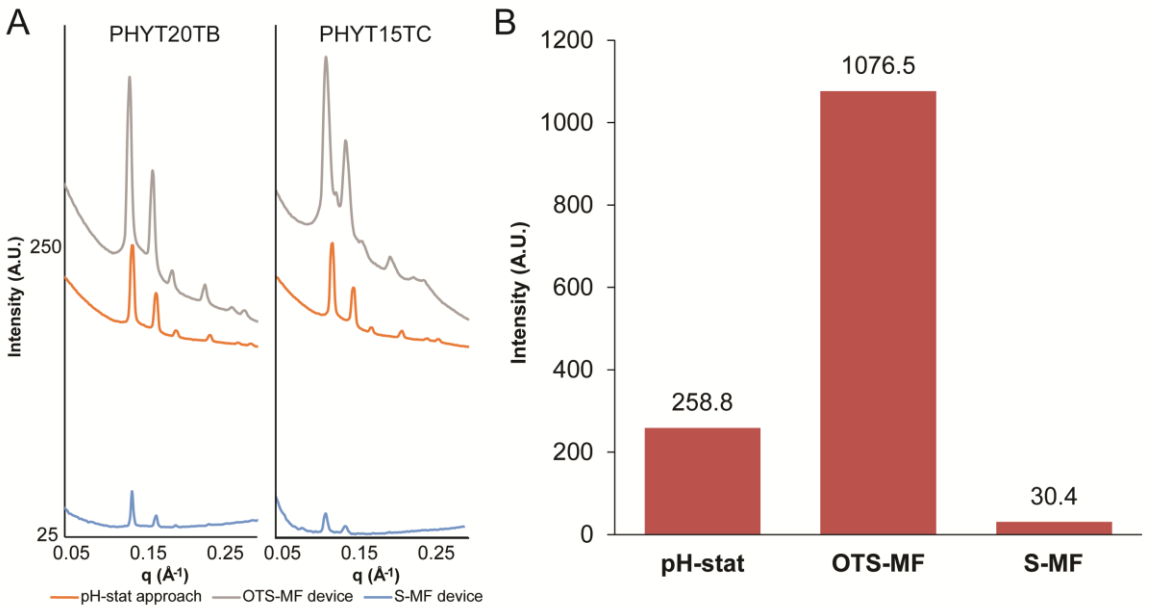

Fig. 7 Comparison of the sensitivity for detection of diffraction peaks of the different devices. A) Scattering profiles of the cubic *Pn3m* phases generated after the digestion of PHYT20TB and PHYT15TC samples within the pH-stat approach, OTS-MF device and S-MF devices (extracted from Fig. 8B),.B) An average of intensities of the first cubic phase peak from the digestions.

As was the case for PHYT20TB, without addition of digestion products the PHYT15TC was an emulsion (L_2 phase) as denoted by the hump as shown in Fig. 6B. The H_2 phase, indicated by the peaks with a spacing ratio of 1, √3 and √4, formed at 9% w/w TC and 6% w/w DP (where in this case DP was 2 mol caprylic acid and 1 mol of monocaprylin) (9TC-6DP). At 3% w/w TC and 12% w/w DP (3TC-12DP), the H_2 phase persisted and the L_2 phase was no longer evident; instead, peaks with relatively low intensity were apparent that indicated the presence of cubic *Pn3m* phase, demonstrated by the minor peaks labelled √2 and √3. Only the cubic *Pn3m* phase remained when all of the TC was replaced with digestion products in the formulation (0TC-15DP). With increasing amount of DP in these static systems, the peak positions were shifting towards lower *q* which correlated with the increase in lattice parameter illustrated in Fig. 6D as the nanoparticles swelled with aqueous phase.

Device sensitivity

To track the structural changes during the digestion of lipid-based formulations, the devices needed to be compatible with SAXS. Ideally, a device composed of X-ray transparent material with thin walls or windows would permit sample detection, and a larger transmission distance/pathlength through the sample would enable greater signal as the X-rays see more scattering material from the sample (but not so thick that multiple scattering effects occur). To determine the relative sensitivity across the three configurations, the signals from the devices are compared in Fig. 7.

The OTS-MF device exhibited high sensitivity for the liquid crystal structures. An X-ray energy setting of 13 keV was sufficient to yield signals from sample within the borosilicate glass capillary. This was expected because the device was constructed from a capillary similar in material and diameter, to the capillaries typically used in experiments for static samples. In fact, it appeared that the OTS-MF capillary yielded at least a three times greater signal than the capillary used in the pH-stat apparatus (Fig. 7B) which could be a result of the microcapillary having a larger capillary diameter and so a greater sample distance.

Comparatively, the S-MF device exhibited a lower sensitivity with SAXS. This is due to the ratio of path length through the sample compared to that through the quartz (or thickness of the sample holder), is much lower than that observed in the OTS-MF device. This required the energy of the X-ray beam to be increased to 20 keV and an additional increase from the usual acquisition time of 5 s to 30 s to counteract the loss of signal. Even after this optimisation, the resultant signal was observed to be about 10 times lower than the standard capillary signals at 13 keV. However, the background signal was also lower, meaning that the diffraction peaks from the sample could still be readily identified.

Kinetic structural evolution during digestion

Kinetics of the phase transitions of PHYT20TB and PHYT15TC were monitored in all three experimental configurations integrated with synchrotron-based SAXS. Fig. 8 displays the scattering profiles obtained from the systems during digestion in the pH-stat approach, OTS-MF device, and S-MF device, while Fig. 9 presents changes in the lattice parameters of the mesophases in the nanoparticles during digestion.

PHYT20TB is a well-studied system that transitions from L_2 phase to the parent cubic *Pn3m* phase during digestion in the pH-stat approach.[4,5] At the start of digestion in the pH-stat approach (Fig. 8A), the *q*-position of the broad hump (indicative of L_2 phase) shifted to the left which suggested the lipid droplets were swelling with water.[37] The shift to lower *q* was also noted between 20TB-0DP and 18TB-2DP for the L_2 phase in Fig. 6A. At approximately 20 secs, two peaks with a spacing ratio of √2 and

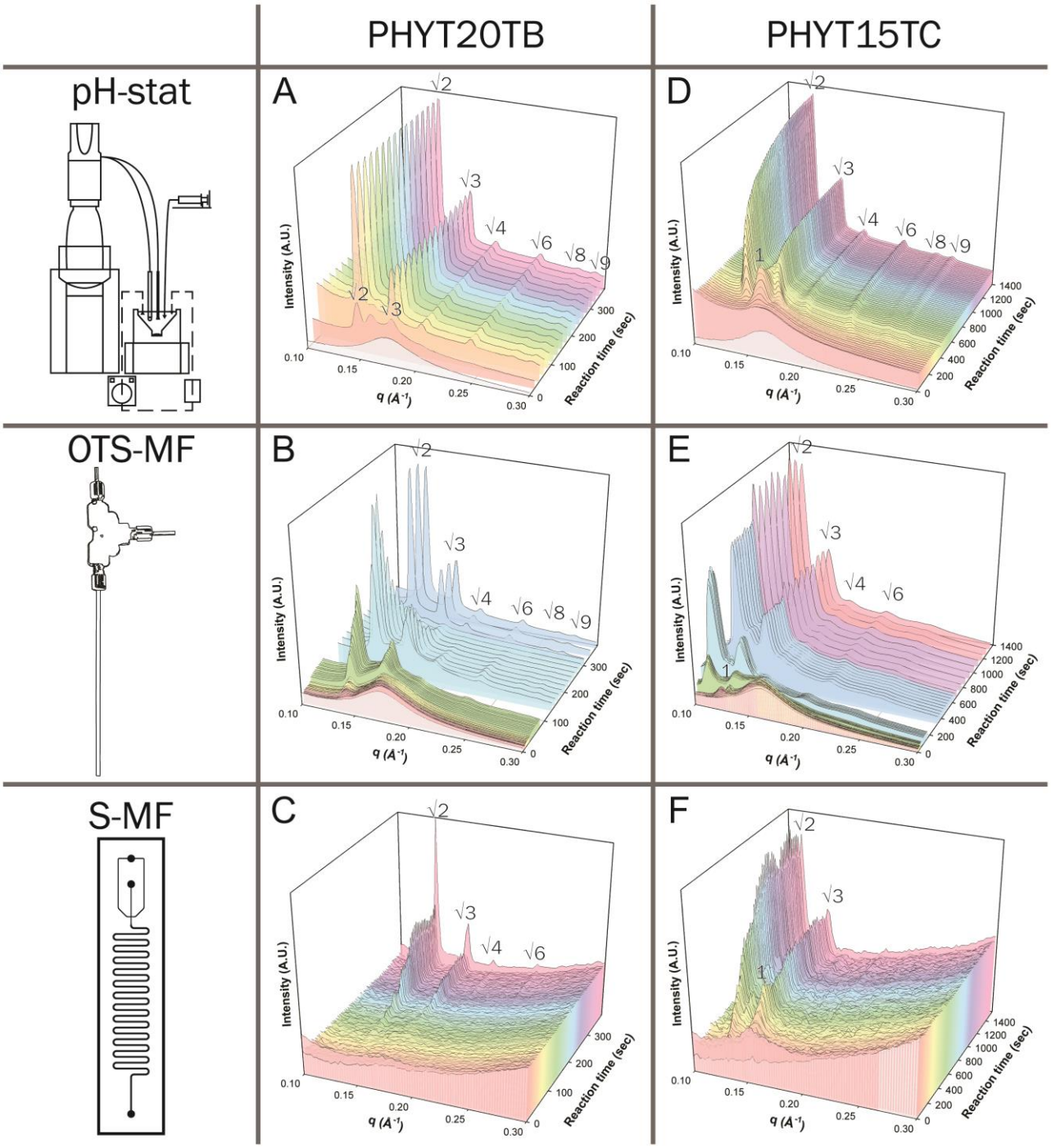

Fig. 8 Tracking the phase transitions with SAXS during the digestion of the emulsion containing phytantriol with 20% w/w tributyrin (PHYT20TB) (A, B, C) and the emulsion containing phytantriol with 15% w/w tricaprylin (PHYT15TC) (D, E, F) in the pH-stat apparatus, OTS-MF and S-MF devices, respectively, illustrated as intensity vs. scattering vector, *q*, plot against time. All six digestions showed a broad hump at time 0, indicative of the unstructured emulsion for PHYT20TB and PHYT15TC. As the formulation underwent digestion, the hump flattened out while other peaks emerged, suggesting a restructuring of the lipid molecules into ordered phases. At the conclusion of all the digestions, at least two peaks were visible in the spacing ratio √2, √3, √4, √6, √8, √9 which is representative of the cubic *Pn3m* phase. For the digestions performed in the OTS-MF device (C, D), experiments performed at the same TFR are grouped with the same colour to differentiate from those done at different TFR.

√3 became visible, sufficient to be identified as cubic *Pn3m* phase.[32] There was a minor amount of cubic phase forming at this stage hence a low intensity signal that was insufficient for the latter peaks (√4, √6, √8, √9 etc.) to be noticeable. Thereafter, the scattering for the cubic *Pn3m* phase remained constant in terms of *q*-position, number of peaks and intensity for the remainder of the digestion where the lattice parameter of the cubosomes in the dynamic digestion was 64.4 Å (Fig. 9A) which was similar to that of 14TB-6DP in Fig. 6A (64.4 Å) indicating that the formulation contained at least 6% w/w digestion products (consisting of glycerol and BA) at that point, which was the

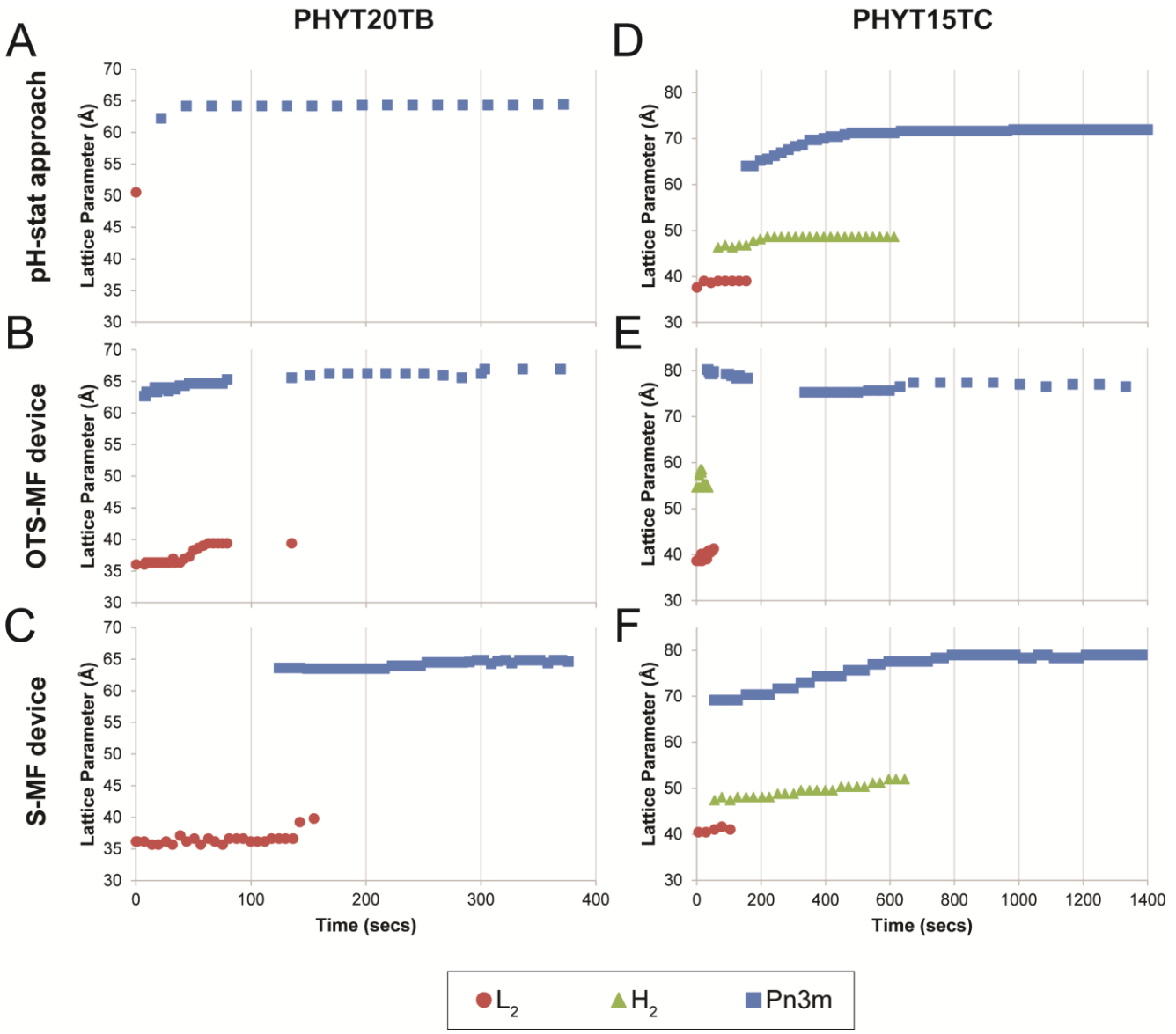

Fig. 9 Tracking the change in lattice parameter (or characteristic distance for the L_2 phase) of the mesophases formed during the digestion of PHYT20TB in the pH-stat method (A), OTS-MF device (B) and S-MF device (C), and PHYT15TC in the pH-stat approach (D), OTS-MF device (E) and S-MF device (F). Lattice parameters were calculated from the peak maxima, and peak broadening was not accounted for.

equivalent of at least 40% digestion. In addition to the cubic phase in the scattering profile at 20 secs, there was an additional peak between the peaks at √2 and √3 at q = 0.155 Å^{-1}. This peak would suggest the coexistence of another structure. No phases aside from L_2 and cubic phases existed in the static samples that represented the various stages of digestion (Fig. 6A). So, it is possible that the peak could be a second *Pn3m* phase with a smaller lattice parameter or an H_2 phase. The exact structure, however, cannot be confirmed given the presence of only one peak. The presence of the unidentified phase in the pH-stat approach may suggest that there was an uneven distribution of the enzyme solution during mixing and the initial transport. A greater proportion of enzyme may have impacted on the packing of the lipids to induce the formation of the intermediate phase. This difference in phase behaviour, although subtle, was also not evident in the data from the literature pH-stat approach,[5] serving to highlight the possible inconsistencies in mixing or lack of resolution associated with studying such transitions when using the pH-stat approach.

Digestion in the OTS-MF device, shown in Fig. 8B, exhibited a relatively smooth transition within each set of TFR (as denoted by the separate colours) however, the sets of kinetic data between the different TFR were noticeably different. The expected phase transition was observed from L_2 to cubic *Pn3m* phase with increasing intensities. However, scattering profiles of adjacent time points from the different sets of TFR were vastly different in regards to the peak heights and peak positions. Between the yellow (6000 µL/hr) and green (2400 µL/hr) sets of data, the first peak for the *Pn3m* phase abruptly increased almost 50% in intensity and the second peak suddenly

became prominent also. The jump in intensity between adjacent time points of different TFR was significantly more pronounced, and it could be due to the large difference in TFR used to compile the kinetic data. The greater difference in TFR would have applied a greater shear stress of the self-assembly of the molecules[38] that appeared to push more structures towards the equilibrium phase earlier in time (or earlier positions in the channel). In Fig. 9B, the digestion yielded cubosomes with a lattice parameter measuring 66.9 Å, which did not correlate exactly with the lattice parameters of the cubic phases in Fig. 6C where the maximum lattice parameter measured was 65.9 Å, which would suggest that the particles formed in this microfluidic device were hydrated to a greater extent as a result of the configuration. The lipase, which was absent in the equilibrium formulations, could have influenced the hydration of the particles.

A smoother transition was observed from L_2 to cubic phase when digested in the S-MF device (Fig. 8C), showing no intermediate phases. The gradual transition as opposed to an almost instantaneous change observed in the pH-stat approach could suggest that the transformation was more controlled with the configuration of the S-MF device. Similar to the pH-stat approach, the lattice parameter of the cubosomes at the last time point reached only 64.6 Å, implying that digestion was at least 40% complete.

Between the digestions of PHYT20TB in the three experimental configurations, the onset of the cubic *Pn3m* phase in the pH-stat approach was the fastest, followed by the OTS-MF device, then the S-MF device. The cubic phase, which is the equilibrium phase after the complete digestion of PHYT20TB, was apparent in the first 20 secs of digestion in the pH-stat approach, and within 12 secs for the OTS-MF device. The lattice parameter for the cubic phase formed in the pH-stat approach (Fig. 9A) remained stable for the remainder of digestion after 40 secs despite at least 40% digestion of the tributyrin which may imply that digestion was complete. The lattice parameter for the cubic phase gradually increased over time during digestion in the OTS-MF device. Interestingly, despite the cubic phase forming quite rapidly in the OTS-MF device, the initial L_2 phase persisted for another 200 secs thereafter. Additionally, the characteristic distance was also trending towards higher values (Fig. 9B) which could suggest that the undigested micelles outside of the sampling range of the X-ray beam may have diffused into this space. The increase in characteristic distance appears logical given that there was a lower concentration of micelles in the sampling range owing to their conversion into cubosomes. This was contrary to the kinetics observed in the S-MF device required only one TFR for the data set where the cubic phase appeared after 120 secs and the lattice parameter of the cubic phases fluctuated slightly (Fig. 9E).

It was previously shown that the PHYT15TC system undergoes a change from L_2 phase to the coexistence of *Pn3m* phase with H_2 phase before completely transforming into the equilibrium *Pn3m* phase of the hydrated lyotropic lipid mixture.[5] When the PHYT15TC emulsion was digested in the pH-stat apparatus (Fig. 8B), a transition from the starting L_2 phase to a broad peak (marked '1') likely to be the first peak indicating the H_2 phase occurred. The broad peak then decayed concurrent with the appearance of peaks at q = 0.137 and 0.168 $Å^{-1}$ (which index at √2 and √3) indicating the formation of cubic *Pn3m* phase particles. The scattering profiles for the cubic phase shifted to lower q indicating the system was taking up water until the first peak for the cubic phase stabilised at q = 0.124 $Å^{-1}$. The attribution of the peak marked '1' to the first H_2 phase peak was inferred from the static samples where the first peak of the H_2 phase was in the same q range (Fig. 6B) and yielding comparable lattice parameters (Fig. 6B and Fig. 9B). The broadening of the peak was likely due to heterogeneous transformations, resulting in the formation of H_2 phase with a range of lattice parameters. This would suggest that the configuration of the pH-stat approach prevented uniform mixing of the enzyme which yielded heterogeneous nanostructures as a consequence. Should an intermediate phase persist for a longer duration as a result of the configurations and not the inherent transformation itself, it would then delay the onset of the subsequent structures also. This would impact on the ability to correlate structures with release behaviour when assessing these systems as potential drug delivery systems. Complete digestion of the TB molecules was also not confirmed *in situ* as the lattice parameter of the cubosomes at the final time point (72.0 Å) did not reach that of the equilibrium systems in Fig. 6D (76.6 Å).

Digestions performed in the OTS-MF device did not exhibit reliable transformations as shown in Fig. 8E**.** Within the first set of kinetic profiles for a TFR of 200 µL/hr (orange), a peak at q = 0.125 $Å^{-1}$ emerged and grew. Although lower than the q range expected for the first H_2 phase peak, it was still suspected that it was H_2 phase but with a larger lattice parameter. In the subsequent TFR (yellow), there was a noticeable decrease in intensity and shift in the q-position of the H_2 phase peak, followed by a sharp transition into cubic *Pn3m* phase in the next TFR (green). The shift in q was evident by the corresponding decrease in lattice parameter of the H_2 phase (Fig. 9E). These unusual variations in peak intensities and lattice parameters between each TFR made it difficult to characterise the kinetics of this system using the OTS-MF device. As with PHYT20TB in the OTS-MF device, this could be attributed to variations in shear stress with different TFR that alter the structural behaviour. Furthermore, the kinetics of this system appeared to exhibit a nonsense order of phase transformations where the H_2 phase disappeared before the disappearance of the L_2 phase, inconsistent with the digestion in literature[5] which could also be attributed to diffusion of the L_2 phase from the bulk flow of the formulation into the collection volume of the X-ray beam.

In contrast to use of the OTS-MF device, the equivalent digestion in the S-MF device exhibited a clear transition from L_2 phase to H_2 phase to cubic phase (Fig. 8F). The improvement in resolution may imply the diffusion-limited digestion of the coaxial flow facilitated a uniform application of the enzyme for more consistent transformations across all particles and droplets in the system, supported by the gradual increase in lattice parameters of the different mesophases present during digestion (Fig. 9F). As particles were able to transform homogeneously, the lattice parameters of the resulting particles were similar which yielded more pronounced Braggs peaks as opposed

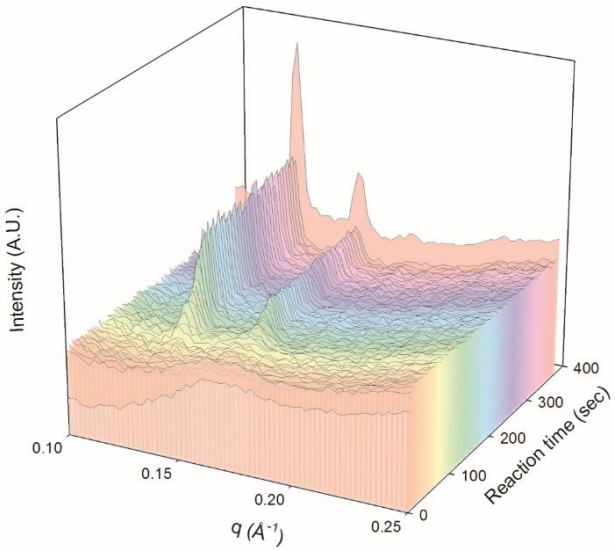

Fig. 10 Digestion of PHYT20TB in the S-MF device with twice the strength of enzyme than the experiment in Fig. 8C. The emergence of the peaks indicative of the cubic *Pn3m* phase occurred at approximately 90 secs. The intensity of the peaks stabilised at a relatively constant height by 150 secs.

to broader peaks. This may indicate that the kinetics observed in the pH-stat approach are in part dictated by the apparatus which is more susceptible to variation in the uniformity of the application of lipase, and therefore, not representative of the system. Digestion of PHYT15TC in the S-MF device produced cubosomes with a lattice parameter (79.0 Å, Fig. 9F) which was approximately 3% greater than the expected dimension from the equilibrium formulations, showing that all TC had digested. However, the mismatch of these corresponding dynamic and equilibrium structure may be attributed to the additional lipase in the dynamic studies.

As the design of the S-MF device facilitated the uniform application of enzyme to the formulation, the activity of the lipase was increased to confirm that enhanced activity would lead to faster rate of reaction on the chip, and therefore faster structural transitions (Fig. 10). When the activity of the lipase was doubled to 1000 TBU/mL of digest, digestion of the PHYT20TB occurred more rapidly. The onset of the peaks indicative of the *Pn3m* phase appeared at approximately the same position on the chip, indicating the same time (~90 secs) as that observed at half the enzyme strength (Fig. 8C). However, the intensity of the peaks stabilised within 150 secs compared to 300 secs for the half-strength digestion. By controlling and limiting the access of lipase to the formulation the kinetics of digestion can be modulated.

Particle size uniformity

When comparing the resulting particle size of the digested liquid crystal nanostructures between the two microfluidic devices, there was no significant difference in the particle size distributions compared to the emulsion prior to digestion (Fig. 11). There was also no difference when compared to the mean particle size of the nanoparticles formed in the equivalent experiments performed in the pH-stat approach, implying that the structured nanoparticles produced after digestion in any of these devices were the same size but the transformation pathway to get there may be different. There was a noticeable increase in variability with results for the pH-stat approach, which could be attributed to some background light scattering by the lipase. The entire system is closed and completely protected

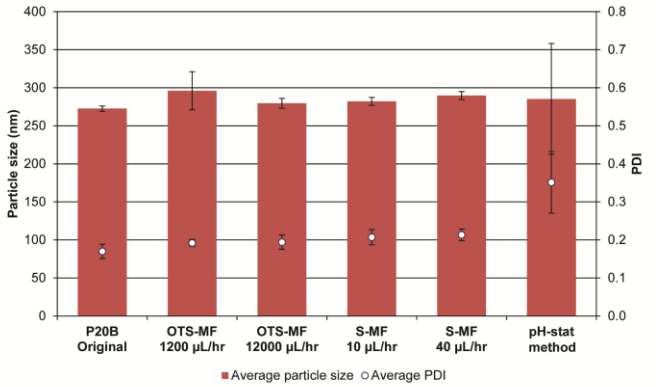

Fig. 11 Particle size of the undigested PHYT20TB emulsion compared to the cubic phase nanoparticles produced during the digestion of PHYT20TB in the S-MF, OTS-MF and pH-stat devices at the specified flow rates. The TFR of the experiments are listed below.

from contamination by dust in the case of microfluidic systems, while the pH-stat approach is open, and opportunistic dust can give rise to larger polydispersity index in dynamic light scattering measurements.

Overall comparison

Microfluidics showed clear improvements to digestion studies in flow when compared to the traditional approach. Integration of the mixing and analysis components overcame problems associated with the separation and transit of materials. In both microfluidic devices, the point of complete mixing occurred sufficiently early in the channels that it did not impede phase transitions. Additionally, factors such as temperature and pH, which were previously controlled in the pH-stat approach and absent in either microfluidic configuration, were found not to exert a significant influence on digestion kinetics which was also a factor concluded by Phan *et al*.[39]

The OTS-MF device could identify phase transitions, however there were inconsistencies in the transition behaviour between different TFR. The transitions were not consistent when changing the flow rate to account for the limited capillary length. This could be due to the different shear stresses applied to the transformation with increasing flow rates as Ghazal *et al.* noted more anisotropy in their liposomes formed above flow rates of 15 µL/min (or 900 µL/hr) in the microchannels.[40] Sections of the capillary were also hidden due to the configuration of the T-junction, therefore a faster flow rate would be required to observe these earlier time points but at the expense of greater sample consumption. The advantage of the device was its simplicity, cost, and its high sensitivity to qualitatively discern the structures. It may also be possible to use a longer length of capillary so that more time points could be collected for any one TFR, however this is dependent on the space limitations with the experimental stage at the synchrotron and availability of commercial capillaries that are sufficiently long and uniform in

diameter.

Although the S-MF device exhibited low sensitivity due to greater absorption of the beam by the quartz housing, it enabled the monitoring of an entire digestion experiment at a fixed flow rate. The thickness of the quartz housing could be further decreased by optimising microfabrication conditions which would increase the sensitivity of the S-MF device. Up to four peaks could be identified for the cubic *Pn3m* phase as opposed to only two observable for the device used in the work by Ghazal *et al.*[12] Additionally, for the S-MF device the >300 mm of channel length allowed the full transformation (of up to 25 mins) to be mapped from the instant the lipase made contact with the formulation through to the endpoint, including the point of complete mixing. Phase transitions in the S-MF device were also slower compared to the digestions performed in the pH-stat approach. The kinetics may be attributed to the lipid stream-enzyme stream interface restricting digestion to a fixed volume of enzyme per volume of lipid. This was not the case with the pH-stat approach where the excess enzyme had access to all the lipid all at once in the mixing vessel so that the mixing efficiency would be unpredictable as solution was continually being drawn up by the peristaltic pump. Mixing was diffusion-limited in the S-MF device and thus more controlled.

Conclusions

By down-scaling the process of the traditional pH-stat approach, the microfluidic process could demonstrate equivalent structural transformations with its simpler and compact design. Between both microfluidic devices, it was clear that the S-MF device produced clearer phase transitions and the whole process could be observed using one TFR, whereas the OTS-MF device necessitated manipulations of the TFR to achieve transformations between phases. Altering flow rates to observe the full phase transformation would introduce variations of shear stress applied to the formation of nanoparticles, which would render inconsistencies within the transformation. In summary, microfluidics using a customized quartz device presents a promising tool that researchers can use for the analysis of their own mixing and kinetic experiments to discriminate phase transitions using in situ SAXS and avoid issues with common materials used in microfluidics such as PDMS. The design also makes the chip suitable to other advanced analytical and spectroscopic techniques.

Conflicts of interest

There are no conflicts to declare.

Acknowledgements

This research was undertaken on the SAXS/WAXS beamline at the Australian Synchrotron, Victoria. Funding is acknowledged from the Australian Research Council under the Discovery Projects scheme DP160102906. BJB is a recipient of an Australian Research Council Future Fellowship (FT120100697). This work was performed in part at the South Australian node of the Australian National Fabrication Facility under the National Collaborative Research Infrastructure Strategy. We would like to also acknowledge Dr. Citsabehsan Devendran, Dr. Jason Brenker and Hanbang Zou from Monash University for their assistance.

Notes and references

1 S. Hyde, B. Ninham, S. Andersson, K. Larsson, T. Landh, Z. Blum and S. Lidin, in *The Language of Shape*, Elsevier, New York, 1997, pp. 199–235.
2 J. Gustafsson, H. Ljusberg-Wahren, M. Almgren and K. Larsson, *Langmuir*, 1997, **13**, 6964–6971.
3 B. Angelov, A. Angelova, V. M. Garamus, S. Lesieur, M. Ollivon, S. Funari, R. Willumeit, P. Couvreur, F.- France, V. Uni and P. Sud, *J. Am. Chem. Soc.*, 2007, **129**, 13474–13479.
4 W. K. Fong, S. Salentinig, C. Prestidge, R. Mezzenga, A. Hawley and B. J. Boyd, *Langmuir*, 2014, **30**, 5373–5377.
5 L. Hong, S. Salentinig, A. Hawley and B. J. Boyd, *Langmuir*, 2015, **31**, 6933–6941.
6 M. Wadsater, J. Barauskas, T. Nylander and F. Tiberg, *Appl. Mater. Interfaces*, 2014, **6**, 7063–7069.
7 S. Salentinig, L. Sagalowicz and O. Glatter, *Langmuir*, 2010, **26**, 11670–11679.
8 J. D. Du, Q. Liu, S. Salentinig, T. H. Nguyen and B. J. Boyd, *Int. J. Pharm.*, 2014, **471**, 358–365.
9 L. Zerkoune, S. Lesieur, J.-L. Putaux, L. Choisnard, A. Geze, D. Wouessidjewe, B. Angelov, C. Vebert-Nardin, J. Doutchh and A. Angelova, *Soft Matter*, 2016, **12**, 7539–7550.
10 B. Angelov, V. M. Garamus, M. Drechsler and A. Angelova, *J. Mol. Liq.*, 2017, **235**, 83–89.
11 B. Angelov, A. Angelova, S. K. Filippov, T. Narayanan, M. Drechsler and S. Petr, *J. Phys. Chem. Lett.*, 2013, **4**, 1959–1964.
12 A. Ghazal, M. Gontsarik, J. P. J. P. Kutter, J. P. Lafleur, A. Labrador, K. Mortensena, A. Yaghmur, K. Mortensen, A. Yaghmur, K. Mortensena and A. Yaghmur, *J. Appl. Crystallogr.*, 2016, **49**, 1–10.
13 A. Yaghmur, P. Laggner, B. Sartori and M. Rappolt, *PLoS One*, 2008, **3**, 1–11.
14 K. Khaliqi, A. Ghazal, I. D. M. Azmi, H. Amenitsch, K. Mortensen, S. Salentinig and A. Yaghmur, *Analyst*, , DOI:10.1039/C7AN00860K.
15 S. Phan, W. K. Fong, N. Kirby, T. Hanley and B. J. Boyd, *Int. J. Pharm.*, 2011, **421**, 176–182.
16 R. Negrini and R. Mezzenga, *Langmuir*, 2011, **27**, 5296–5303.
17 J. Khan, T. Rades, B. Boyd and B. Boyd, *Pharm. Res.*, 2016, **33**, 548–562.
18 D. B. Warren, M. U. Anby, A. Hawley and B. J. Boyd, *Langmuir*, 2011, **27**, 9528–9534.
19 J. Barauskas and T. Landh, *Langmuir*, 2003, **19**, 9562–9565.
20 I. U. Khan, C. A. Serra, N. Anton and T. Vandamme, *J. Control. Release*, 2013, **172**, 1065–1074.
21 N. Rott, *Annu. Rev. Fluid Mech.*, 1990, **22**, 1–11.
22 S. With, M. Trebbin, C. B. A. Bartz, C. Neuber, M. Dulle, S. Yu, S. V Roth, H.-W. Schmidt and S. Forster, *Langmuir*, 2014, **30**, 12494–12503.
23 H. Song, J. D. Tice and R. F. Ismagilov, *Angew. Chemie - Int. Ed.*, 2003, **42**, 768–772.

24 A. Ghazal, J. P. Lafleur, K. Mortensen, J. P. Kutter, L. Arleth and G. V. Jensen, *Lab Chip*, 2016, **16**, 4263–4295.
25 A. Otten, S. Köster, B. Struth, A. Snigirev and T. Pfohl, *J. Synchrotron Radiat.*, 2005, **12**, 745–750.
26 E. Bottaro and C. Nastruzzi, *Mater. Sci. Eng. C*, 2016, **64**, 29–33.
27 A. Terray and S. J. Hart, *Lab Chip*, 2010, **10**, 1729.
28 H.-S. Wu and M.-J. Tsai, *Enzyme Microb. Technol.*, 2004, **35**, 488–493.
29 L. Sek, C. J. H. Porter and W. N. Charman, *J. Pharm. Biomed. Anal.*, 2001, **25**, 651–661.
30 A. J. A. J. Clulow, M. Salim, A. Hawley and B. J. B. J. Boyd, *A closer look at the behaviour of milk lipids during digestion*, Elsevier, 2017.
31 S. T. Mudie, ScatterBrain.
32 S. T. Hyde, in *Handbook of Applied Surface and Colloid Chemistry*, ed. K. Holmberg, John Wiley & Sons, Ltd, 2001, pp. 299–332.
33 N. M. Kirby, S. T. Mudie, A. M. Hawley, D. J. Cookson, H. D. T. Mertens, N. Cowieson and V. Samardzic-Boban, *J. Appl. Crystallogr.*, 2013, **46**, 1670–1680.
34 J. P. Brody, P. Yager, R. E. Goldstein and R. H. Austin, *Biophys J*, 1996, **71**, 3430–3441.
35 J. Donnér, *Acta Chem. Scand.*, 1976, **30**, 430–434.
36 D. Dutta, A. Ramachandran and D. T. Leighton, *Microfluid. Nanofluidics*, 2006, **2**, 275–290.
37 N. B. Bisset, B. J. Boyd and Y. Da Dong, *Int. J. Pharm.*, 2015, **495**, 241–248.
38 C. R. Safinya, E. B. Sirota and R. J. Plano, *Phys. Rev. Lett.*, 1991, **66**, 1986–1989.
39 S. Phan, S. Salentinig, A. Hawley and B. J. Boyd, *J. Pharm. Sci.*, 2015, **104**, 1311–1318.
40 A. Ghazal, M. Gontsarik, J. P. Kutter, J. P. Lafleur, D. Ahmadvand, A. Labrador, S. Salentinig and A. Yaghmur, *J. Phys. Chem. Lett.*, 2016, 73–79.

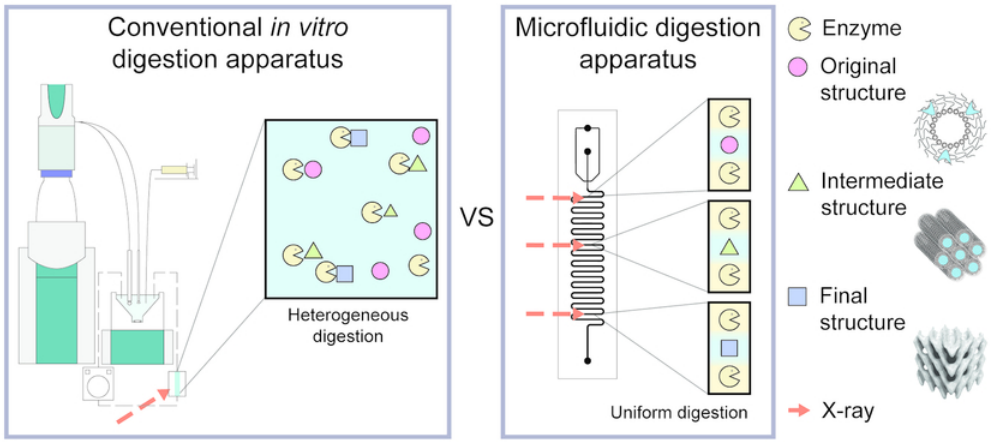

Microfluidics affords more control over transformations than current setups to monitor the digestion of lipid-based formulations with X-ray scattering techniques.

70x35mm (300 x 300 DPI)